Available online at www.sciencedirect.com
ScienceDirect
Atmospheric Environment 41 (2007) 4865–4876
ATMOSPHERIC ENVIRONMENT
www.elsevier.com/locate/atmosenv

Variations of the increasing trend of tropospheric NO_2 over central east China during the past decade

Youjiang He[a,*], Itsushi Uno[b], Zifa Wang[c], Toshimasa Ohara[d], Nobuo Sugimoto[d], Atsushi Shimizu[d], Andreas Richter[e], John P. Burrows[e]

[a]*Earth System Science and Technology, Kyushu University, Fukuoka, Japan*
[b]*Research Institute for Applied Mechanics, Kyushu University, Fukuoka, Japan*
[c]*Institute of Atmospheric Physics, Chinese Academy of Science, Beijing, China*
[d]*National Institute for Environmental Studies, Tsukuba, Ibaraki, Japan*
[e]*Institute of Environmental Physics, University of Bremen, Bremen, Germany*

Received 2 October 2006; received in revised form 5 February 2007; accepted 6 February 2007

Abstract

A numerical analysis using a regional chemical transport model (CTM) is presented in comparison with Global Ozone Monitoring Experiment (GOME) and SCanning Imaging Absorption spectroMeter for Atmospheric CHartographY (SCIAMACHY) satellite NO_2 measurements over East Asia from 1996 to 2005 from a climatological perspective. Modeling results agree well with satellite retrievals in geographical distribution patterns, with systematic underestimation of the absolute values. The sharp increase in NO_2 vertical column densities (VCDs) over central east China (CEC) after the year 2000 (14.1–20.5% yr^{-1} for the satellite observations and 10.8% yr^{-1} for model simulations) is analyzed quantitatively over different megacity clusters. The distinct emission increase patterns are responsible for the different increase trends observed over the Beijing megacity cluster (BJ), the Yangtze Delta (YD) and other CEC regions. The growth rate of satellite measured and CMAQ-modeled NO_2 VCDs for the YD is much higher than that in other regions, with no clear seasonal variation. Apart from BJ and YD, NO_2 emissions from other regions in CEC also expand considerably.

Keywords: Tropospheric NO_2; Increasing trend; NO_x emission; Satellite; Central east China

1. Introduction

Tropospheric NO_2 plays an important role in atmospheric chemistry. Concomitant with the rapid economic development, tropospheric NO_2 pollution over East Asia has kept a persistent increase since the 1970s and even surpassed the emissions from North America and Europe until mid-1990s (Akimoto, 2003). In addition, Aardenne et al. (1999) estimated Asian NO_x emissions to increase by 350% to 85.6 Tg during 1990–2020, which is expected to influence the contribution to future wet deposition and long-range transport of nitrogen-containing acids over northeastern Asia (Kim and Cho, 2003). Tropospheric vertical column densities (VCDs) of NO_2 retrieved from measurements of the

*Corresponding author. Tel.: +81 92 583 7773; fax: +81 92 583 7774.
E-mail address: yjhe@riam.kyushu-u.ac.jp (Y. He).

1352-2310/$ - see front matter © 2007 Elsevier Ltd. All rights reserved.
doi:10.1016/j.atmosenv.2007.02.009

Global Ozone Monitoring Experiment (GOME) have been combined with other tools to describe the regional and temporal variability of NO_2 emissions, distribution and abundance (e.g. Leue et al., 2001; Richter and Burrows, 2002; Martin et al., 2003). Richter et al. (2005) pointed out the continuous and marked increase in tropospheric NO_2 abundance over central east China (CEC; 30°N–40°N, 110°E–123°E) during 1996–2004 using GOME and SCanning Imaging Absorption spectroMeter for Atmospheric CHartographY (SCIAMACHY) NO_2 measurements. Irie et al. (2005) also confirmed the growth trend of tropospheric NO_2 over CEC using the same GOME results and ground-based UV/VIS spectrometer observations. Van der A et al. (2006) detected the considerable growth of tropospheric NO_2 over eastern China, especially above industrial areas such as Shanghai that have shown rapid economical growth. That study revealed different seasonal patterns of NO_2 concentration with the maximum during winter over eastern China and the maximum in summer over western China.

Chemical transport models (CTMs) are one of the most important tools to quantitatively evaluate the spatial and temporal distribution of trace constituents and controlling processes of their budgets in the atmosphere. Several CTMs have been combined with GOME NO_2 to investigate its retrieval and behaviors. Kunhikrishnan et al. (2004) validated the enhancement of GOME-retrieved NO_2 abundance over China, especially for industrial regions, with a CTM model. Velders et al. (2001) showed that model simulated tropospheric NO_2 shows the same order of magnitude and pattern as GOME retrievals over industrialized areas of the United States and Europe, but presents a factor of 2–3 lower over China. Ma et al. (2006), van Noije et al. (2006) and Uno et al. (2007) achieved similar results using different CTMs. However, more extensive analysis of long-term regional CTM model simulations with tropospheric NO_2 retrievals from satellite measurements is necessary for different areas over CEC to elucidate the reasons for such discrepancies.

In contrast to previous studies, this paper presents a comparison of 10-year regional CTM modeling results from 1996 to 2005 with NO_2 measurements derived from GOME and SCIAMACHY in a climatological perspective, with particular emphasis on the sharply increasing trend of observed NO_2 VCDs over CEC since 2001 and the discrepancies between model results and satellite retrievals.

2. Data sources and methodology

2.1. GOME and SCIAMACHY retrievals

GOME is an instrument on board the ERS-2 satellite that provides data with a resolution of 40 km (latitude) × 320 km (longitude) since June 1995. The ERS-2 satellite crosses the equator at 10:30 local time in a sun-synchronous polar orbit and achieved global coverage every 3 days until June 2003 (e.g., Burrows et al., 1999; Richter and Burrows, 2002; Boersma et al., 2004). After that time, GOME coverage is reduced as a result of permanent failure of the last tape recorder on ERS-2. Here, we use the version 2 GOME NO_2 data from the University of Bremen that is described in Richter and Burrows (2002) and Richter et al. (2005) and was validated by Ordóñez et al. (2006).

SCIAMACHY launched on board the ENVISAT satellite in March 2002 provides NO_2 VCDs data with improved spatial resolution of 60 × 30 km since August 2002. The retrieval algorithm is similar to that used for GOME data and is described by Richter et al. (2005). SCIAMACHY NO_2 VCDs has been validated by comparing with airborne in situ measurements in eastern America (Martin et al., 2006) and southern Europe (Heue et al., 2005). The bias between GOME and SCIAMACHY was proven to be negligible and with no latitudinal dependence (van der A et al., 2006). Therefore, we combined GOME (1996–2002, ver. 2) and SCIAMACHY (2003–2005, ver. 0.7) data to obtain a continuous time series of NO_2 abundance over East Asia for 10 years.

2.2. Model description and emission inventory

The regional CTM used in this study was developed jointly by Kyushu University and the National Institute for Environmental Studies (Uno et al., 2005) based on the Models-3/Community Multiscale Air Quality (CMAQ, ver. 4.4) modeling system released by the US EPA. Briefly, the model is driven by meteorological fields that are generated by the Regional Atmospheric Modeling System (RAMS) with initial and boundary conditions defined by NCEP reanalysis data. The model has been successfully applied for Asian air quality studies by Uno et al. (2005) and Tanimoto et al. (2005).

Reliable emission inventories of air pollutants are becoming increasingly important to assess heavy air

pollution problems in Asia. The Regional Emission inventory in Asia (REAS; Ohara et al., 2006; Akimoto et al., 2006), which is based on several energy statistics, emission factors and other socio-economical information between the years 1980 and 2003, is used in this study. REAS emission data are distributed into a $0.5^\circ \times 0.5^\circ$ grid using index databases of population, locations of large point sources (LPS), road networks and land coverage information. Among REAS, NO_x emission inventory mainly consists of fossil fuel and biofuel combustions. Biomass burning NO_x emission is also involved. REAS soil NO_x emission (sum of N-fertilized soil and natural soil) is estimated to be 400–500 Gg N yr^{-1} from China, which is approximately 12–15% of combustion base NO_x and is highly uncertain. So soil NO_x emission is not considered in this research. Lighting NO_x emission is also not included at present.

2.3. Model settings and experiment design

The horizontal model domain for the model is $6240 \times 5440\,km^2$ on a rotated polar stereographic map projection centered at 25°N, 115°E with $80 \times 80\,km^2$ grid resolution. For vertical resolution, 14 layers exist in the sigma-z coordination system up to 23 km, with about seven layers within the boundary layer below 2 km. The SAPRC-99 scheme is applied for gas-phase chemistry. We performed 10 full calendar year simulations during 1996–2005 with the initial fields and monthly averaged lateral boundary condition for most chemical tracers provided by a global CTM (CHASER; Sudo et al., 2002). Except for biomass burning NO_x emission, of which the discussion about the seasonality is described by Streets et al. (2003), seasonal emission variation is not considered in the simulation. Model output data are interpolated to $0.5^\circ \times 0.5^\circ$ resolution as REAS to facilitate an easy comparison. The same has been done with GOME- and SCIAMACHY-retrieved data.

Two sets of numerical experiments were conducted with year-by-year meteorology: one with emissions fixed to those of the year 2000 (E00Myy) and the other with year-by-year emission of REAS (EyyMyy). As REAS only provides emission inventories up to the year 2003, we used the fixed emissions of the year 2003 to represent the following years in the experiment (EyyMyy). Quantitative and systematic analysis of the two experiments' output is performed to examine the impacts of emission increase and meteorology on the regional pattern change of NO_2 VCDs over CEC in the past 10 years. Because the GOME and SCIAMACHY measurements in low and middle latitudes are always taken at the same LT (approximately 10:30 LT and 10:00 LT, respectively), we use model output data of three UTC (11:00 LT for China). To obtain NO_2 VCDs comparable to the satellite retrievals, we integrated the column loading from the surface to 10 km altitude without considering seasonal variation of tropopause height, which is acceptable as approximately 95% of NO_2 resides at altitudes below 3 km in CMAQ simulations. In this paper we only focused on CEC, the same region as that addressed in Richter et al. (2005) as shown in Fig. 1. Two megacity cluster regions within CEC are selected: the Beijing and surrounding region (BJ; 114–118.5°E, 36–40°N) and the Yangtze Delta (YD; 118–122°E, 30–32.5°N). The remaining part of the CEC, which includes a number of urban cities and wide rural areas, is denoted as RC.

3. Results and discussion

3.1. Comparison of model results with satellite retrievals

Uno et al. (2007) systematically examined our model results for East Asia using GOME retrievals. The present study specifically addresses validation of model results using GOME and SCIAMACHY retrievals over CEC region. Figs. 1a and b, respectively, present the SCIAMACHY retrieved and CMAQ modeled geographical distribution of annual mean tropospheric NO_2 VCDs over East Asia for 2003. In general, model simulations agree well with SCIAMACHY observations in geographical distribution patterns for the relatively high NO_2 VCDs regions over CEC, northeast China, western Korea and central Japan. Model results even clearly show hot spots over Beijing, the YD, the Pearl River delta, Seoul, Pusan and Tokyo. Within the CEC region, as a result of varying development levels and different structure of industry, economy and energy production, NO_2 VCDs are much higher over BJ and YD but comparatively lower over the RC region. Scatter plots showing modeling results and SCIAMACHY retrievals for these three regions are shown in Fig. 1c with different notation. With respect to SCIAMACHY retrievals, the model simulation

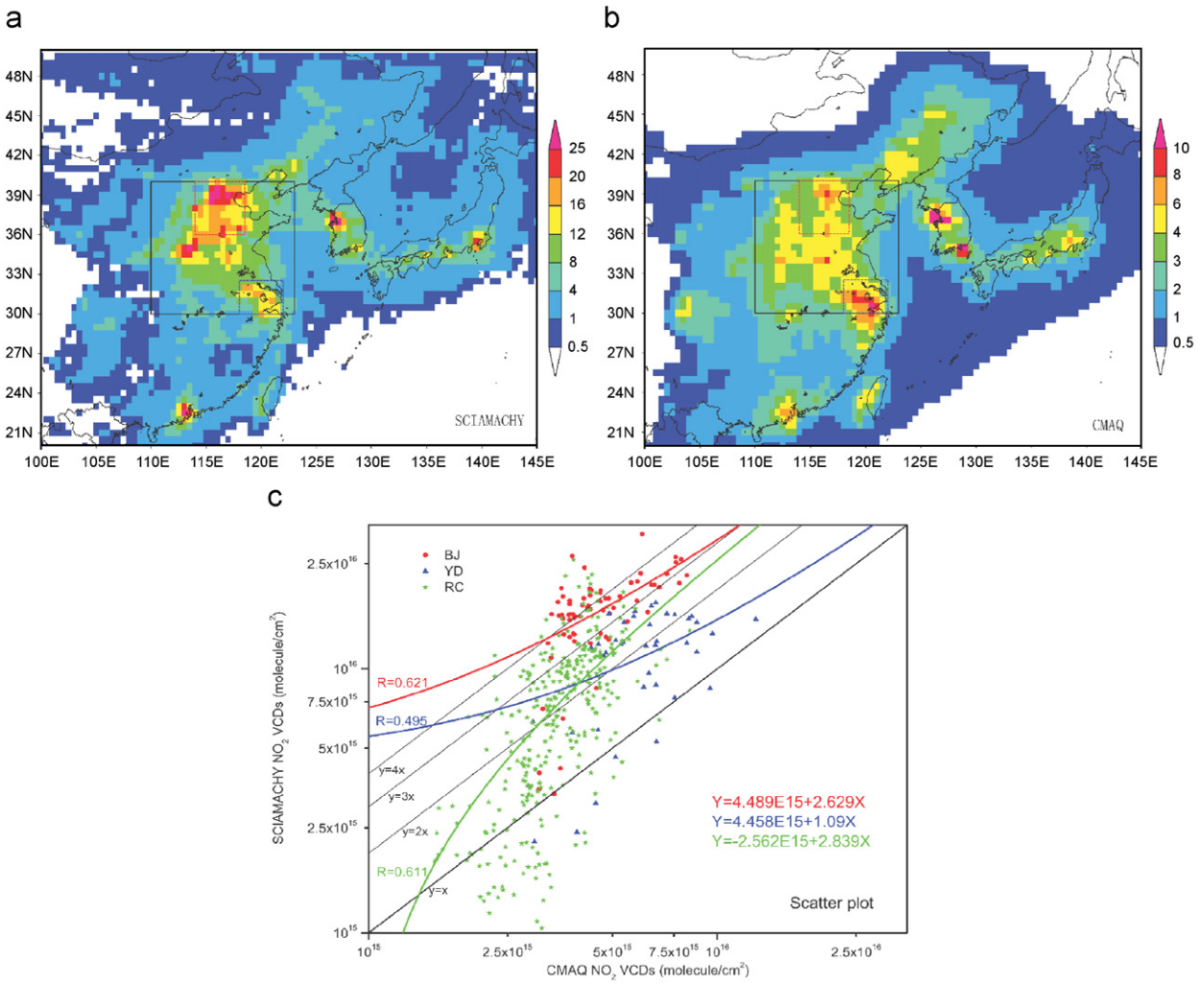

Fig. 1. Comparison of CMAQ-simulated and SCIAMACHY-observed annual mean NO_2 VCDs in 2003. (a) CMAQ simulations (unit: 1E15 molecule cm^{-2}), (b) SCIAMACHY retrievals (unit: 1E15 molecule cm^{-2}) and (c) scatter plots of annual mean NO_2 VCDs between CMAQ (set as x) and SCIAMACHY (set as y) over CEC. In Fig. 1a and b, black line square represents CEC (110–123°E, 30–40°N); the red dashed line square represents Beijing and surrounding regions (BJ; 114–118.5°E, 36–40°N), blue dashed line square represents the Yangtze Delta (YD; 118–122°E, 30–32.5°N). In (c) red circles, blue triangles and green stars represent BJ, YD and RC, respectively.

systematically underestimates the tropospheric NO_2 abundance in almost all areas in CEC. Most points of the SCIAMACHY retrieval data are almost 3–4 times higher than model results over BJ, as shown by red circles and the regression line, and 1–3 times higher over YD, as shown by blue triangles and the regression line. The ratio between SCIAMACHY retrievals and CMAQ simulations for all points in RC spans a wide range from less than 1 to more than 4. The grid points with a ratio of more than 4 were found to be situated in the coal thermal power plant regions. Those with a ratio of less than 1 come from rural regions, which are responsible for the distinct linear correlation suggested in Fig. 1c between RC and BJ/YD. In general, similar to the results presented in Velders et al. (2001), Ma et al. (2006) and van Noije et al. (2006), our model results agree well with SCIAMACHY retrievals for YD and RC with a similar systematic underestimation factor of 1–3. The unexpectedly large underestimation of NO_2 VCDs over BJ with respect to SCIAMACHY retrievals is probably due to the rapid development of traffic in recent years.

3.2. Sharply increasing trend of tropospheric NO_2 abundance since 2001

As reported by Richter et al. (2005), a continuous increase of NO_2 VCDs is apparent over CEC with accelerating growth of 4% yr^{-1} in 1997 and 12% yr^{-1} in 2002. In the present study, we particularly examine the sharp increase in NO_2 abundance since 2001. Monthly and annual mean satellite- measured and model-simulated tropospheric NO_2 VCDs over CEC are shown in Fig. 2. The relative annual growth rate during two different stages is shown in Table 1 (DJF represents December, January and February). During 1996–2005, satellite-measured annual NO_2 VCDs over CEC increased about 7.2×10^{15} molecule cm^{-2}, which is more than twice that of 1996. During 2001–2005, the annual increase rate of the satellite retrievals abruptly increased to 20.5%, although it was approximately 6.7% during 1996–2000. The growth rate is much higher in winter, with satellite-measured NO_2 VCDs in January 2005 being nearly three times as large as that in January 1996.

Model simulations systematically underestimate tropospheric NO_2 VCDs compared with satellite retrievals over CEC. Therefore, in Fig. 2, the vertical axis for CMAQ (right axis) is adjusted to produce a better view. It is exciting to note that model simulations (EyyMyy) not only reproduce the mild increase in NO_2 VCDs during 1996–2000 with an annual increase rate of 1.7% but also successfully capture the increased annual growth rate of 10.8% from 2001 to 2003, which is slightly lower than that of satellite retrievals with 14.1% yr^{-1} (2000–2003). Modeled (EyyMyy) NO_2 abundance shows no marked increase tendency after 2004 as the emissions were fixed to those of 2003. In contrast, the annual mean modeled (E00Myy) NO_2 VCDs, which use constant emissions, show no clear tendency toward increase. They show only small fluctuations during those 10 years. The distinction between the EyyMyy and E00Myy simulations highlights the dominant role of emission increase in the accelerating growth of tropospheric NO_2 over CEC.

Simulation results (EyyMyy) well capture satellite-observed increasing NO_2 VCDs in summer and also reproduce the greatly increased trend in winter from 1996 to 2003. It is noteworthy that modeled (EyyMyy) monthly mean values fail to reflect the satellite-measured high peaks in winter after 2000. Table 1 shows that the annual REAS emission increase rate of 10.4% yr^{-1} is much lower than the satellite-observed annual growth rate, especially for winter of 20.1% during 2000–2003 over CEC. During that period, model simulation (EyyMyy) shows a growth rate of 10.8% yr^{-1} for annual mean data and 12.1% yr^{-1} for winter, which closely resembles the emission growth rate because of the short lifetime of NO_2. Additionally, the growth rate of NO_2 abundance in winter and other seasons is similar for model simulation (EyyMyy) but much different for satellite retrievals with a much higher linear growth rate of 20.1% yr^{-1} in winter and a

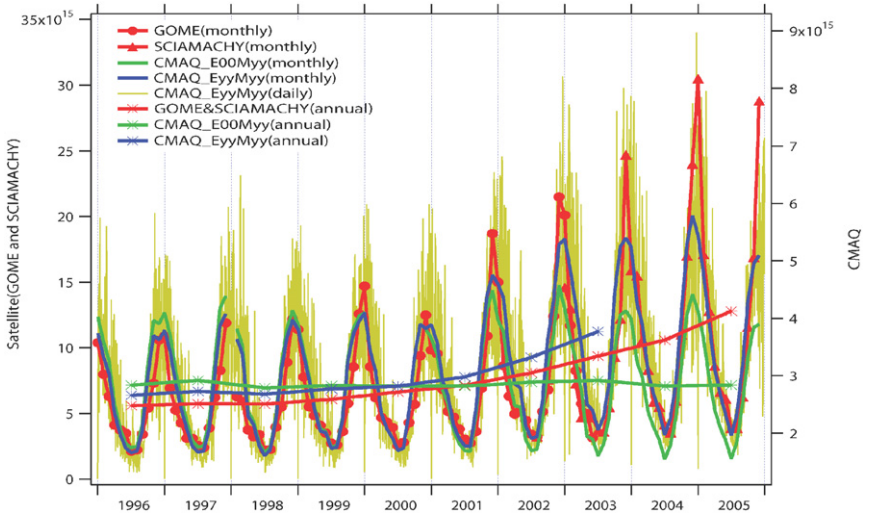

Fig. 2. Time series of satellite observed and model simulated annual and monthly mean NO_2 VCDs during 1996–2005 over CEC (unit: molecule cm^{-2}). Red lines represent satellite observations, and other colored lines represent model simulations.

Table 1
Emission amount of NO_x and the annual increase rate (%) of satellite-measured and CMAQ-modeled NO_2 VCDs over Central East China

Region	Emissions (Tg yr^{-1})		Annual increase rate (% yr^{-1})							
	REAS (2000)	TRACE-P (2000)	Stage	REAS	GOME/SCIAMACHY				CMAQ/REAS	
					Annual	Winter (DJF)	March–November	Annual	Winter (DJF)	March–November
CEC	4.6	4.8	I	2.1	6.7	7.3	3.6	1.7	2.1	1.5
			II	10.4	14.1/20.5	20.1/25.2	9.9/16.8	10.8	12.1	10.2
BJ	1.1	1.1	I	2.2	10.5	12.3	6.3	1.5	1.5	1.4
			II	9.1	14.3/23.1	21.1/24.2	9.2/22.2	10.7	14.0	9.5
YD	0.9	0.8	I	4.2	5.0	5.8	2.8	5.7	5.7	5.6
			II	8.2	17.6/27.5	17.3/25.8	17.7/29.0	8.2	7.9	8.5
RC	2.6	2.9	I	1.3	5.6	5.9	2.8	1.2	1.6	1.0
			II	11.8	14.5/18.4	22.1/26.0	9.3/13.4	11.5	12.9	10.8

Note: Stage I represents period 1996–2000; stage II represents period 2000–2003/2000–2005 for GOME and SCIAMACHY and period 2000–2003 for CMAQ. Growth rate is determined from linear regression.

lower value of 9.9% yr^{-1} in other seasons during that period.

Fig. 3 shows NO_2 absolute concentrations and the relative contributions of the three regions within CEC as a 3-month moving average. The red line represents satellite retrievals and the blue line shows modeling results. Good correlation is found with interannual and seasonal variations for the YD and RC region: the linear regression equations for CMAQ NO_2 (x) and GOME NO_2 (y) VCDs are the following for 1996–2003.

$$\mathrm{YD}: y = -2.58\mathrm{E}15 + 2.16x \ (R = 0.86),$$

$$\mathrm{RC}: y = -3.57\mathrm{E}15 + 3.56x \ (R = 0.90).$$

Nevertheless, a poor correlation is apparent for BJ because CMAQ cannot reproduce the sharp winter peak over this region.

The average relative contributions from BJ, YD and RC to CEC are about 26%, 12% and 62%, respectively, for GOME/SCIAMACHY measurements, and around 20%, 15% and 65% for CMAQ/REAS simulations. This also indicates that CMAQ simulations underestimate the contribution from BJ and slightly overestimate those of YD and RC compared with satellite retrievals. Fig. 3 also shows, that for the satellite measurements, the relative contribution is increased for BJ in winter, but decreased for YD and RC. This indicates that BJ contributes more to the satellite-measured high peaks in winter than in other seasons over CEC, while YD and RC contribute more in other seasons. In the satellite data, the relative contribution from BJ has increased markedly since 2001 when the sharp increase is observed. While at the same time the contribution from RC decreased. This feature suggests that BJ dominates the rapid increase of NO_2 VCDs measured by satellite since 2001. In contrast to the satellite observations, in the CMAQ simulations (EyyMyy), YD and RC contribute much to the high peaks of NO_2 VCDs over CEC in winter when the relative contribution increased for YD and RC while decreased for BJ. The difference in the relative contributions indicated by satellite and model results might indicate that the model simulation underestimates the NO_2 abundance over BJ much more than in other regions. The non-seasonal fossil fuel and biofuel combustion NO_x emission used in CMAQ might be one reason for this underestimation, especially in winter over the BJ region (the effect of seasonality of emission was estimated to be approximately 1.2 between maxima and minima value by Streets et al., 2003).

3.3. NO_2 growth rate based on the monthly variation of NO_2 abundance of year 2000

Fig. 4 presents satellite- measured and model-simulated monthly time series of the growth of NO_2 abundance (calculated by the difference from the monthly variation of NO_2 abundance of year 2000), over BJ, YD and RC, respectively. Satellite-measured increase percentages (SIP) of NO_2 abundance, CMAQ-modeled absolute increment (MAI) and the

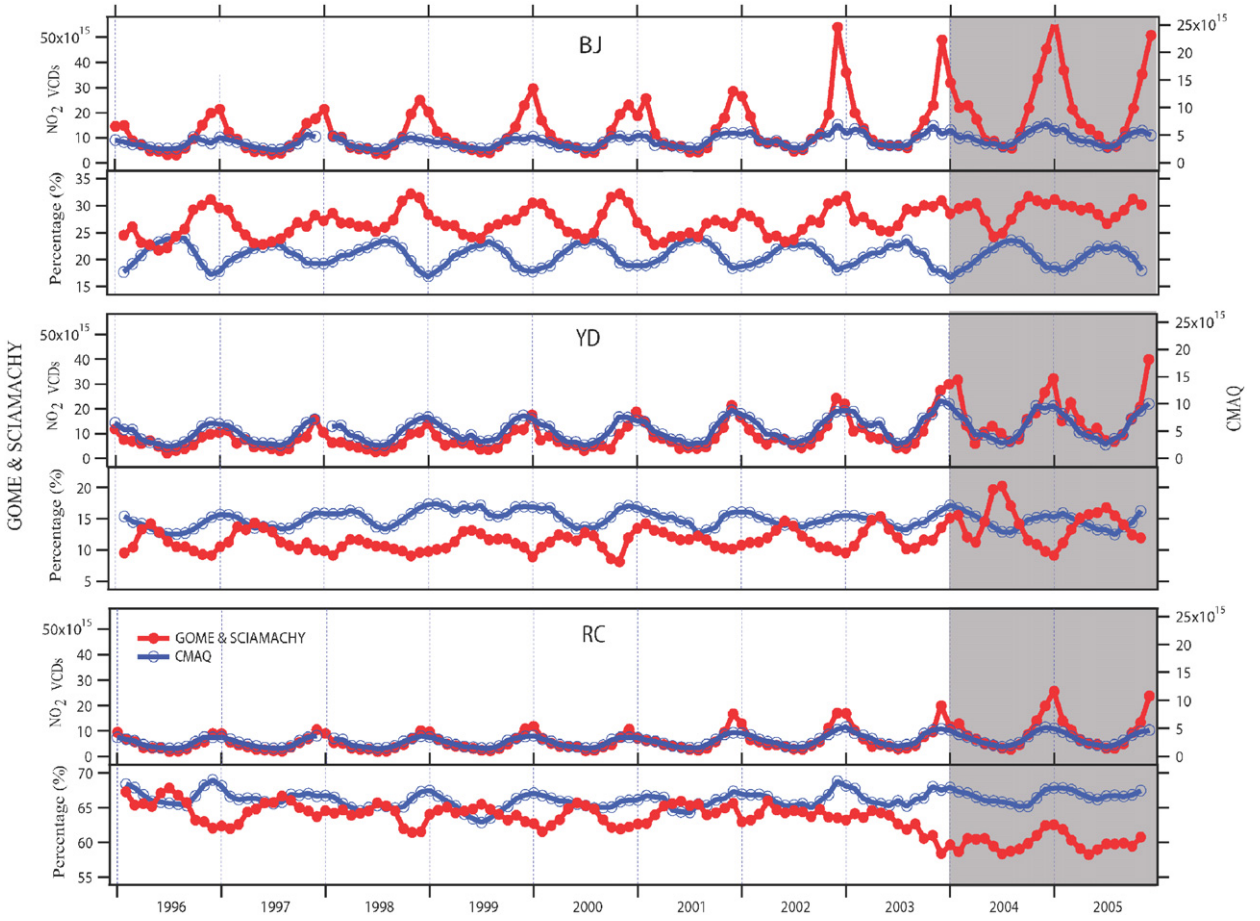

Fig. 3. (Upper) Time series of satellite-measured and CMAQ-modeled NO_2 VCDs (unit: molecule cm^{-2}); (lower) the relative contribution rate of NO_2 abundance over BJ, YD and RC to mean NO_2 VCDs over CEC. Red lines represent satellite observations; blue lines represent model simulations. Model simulations with fixed emissions of 2003 for 2004–2005 are masked with shadow.

increase percentage (MIPE) caused by emission increase based on the monthly variation of NO_2 abundance of year 2000 are calculated as

$$\mathrm{SIP}(\%) = (\mathrm{Satellite}_{yy} - \mathrm{Satellite}_{00}) \times 100/\mathrm{Satellite}_{00},$$

$$\mathrm{MAI} = (\mathrm{CMAQ}_{\mathrm{EyyMyy}} - \mathrm{CMAQ}_{\mathrm{E00Myy}})$$

and

$$\mathrm{MIPE}(\%) = (\mathrm{CMAQ}_{\mathrm{EyyMyy}} - \mathrm{CMAQ}_{\mathrm{E00Myy}}) \times 100/\mathrm{CMAQ}_{\mathrm{E00M00}},$$

where $\mathrm{Satellite}_{yy}$ and $\mathrm{Satellite}_{00}$, respectively, represent satellite retrievals for each year and for the year 2000. The SIP represents the monthly growth rate of satellite-measured NO_2 abundance. Whereas the MAI presents the absolute increment of CMAQ-modeled NO_2 VCDs caused mainly by the emission increase; MIPE reflects the monthly growth rate of modeled NO_2 VCDs caused chiefly by the increase in emission.

Compared with the year 2000, SIP shows a marked increase during 2001–2005 for each region, with the highest growth rate shown over YD, as depicted in Fig. 4a. Fig. 4b shows that the satellite-measured increase in NO_2 VCDs over the three regions is also reflected by the model-simulated absolute increment NO_2 VCDs that is mainly attributable to the increase in emission. MAI maintains a continuous increase during the past 10 years and presents more conspicuous growth during 2000–2003 over all regions, with the highest value over YD. van der A et al. (2006) observed a considerable increase in $20 \pm 6\%\ \mathrm{yr}^{-1}$ in the period 1996–2005 for Shanghai, which is consistent with

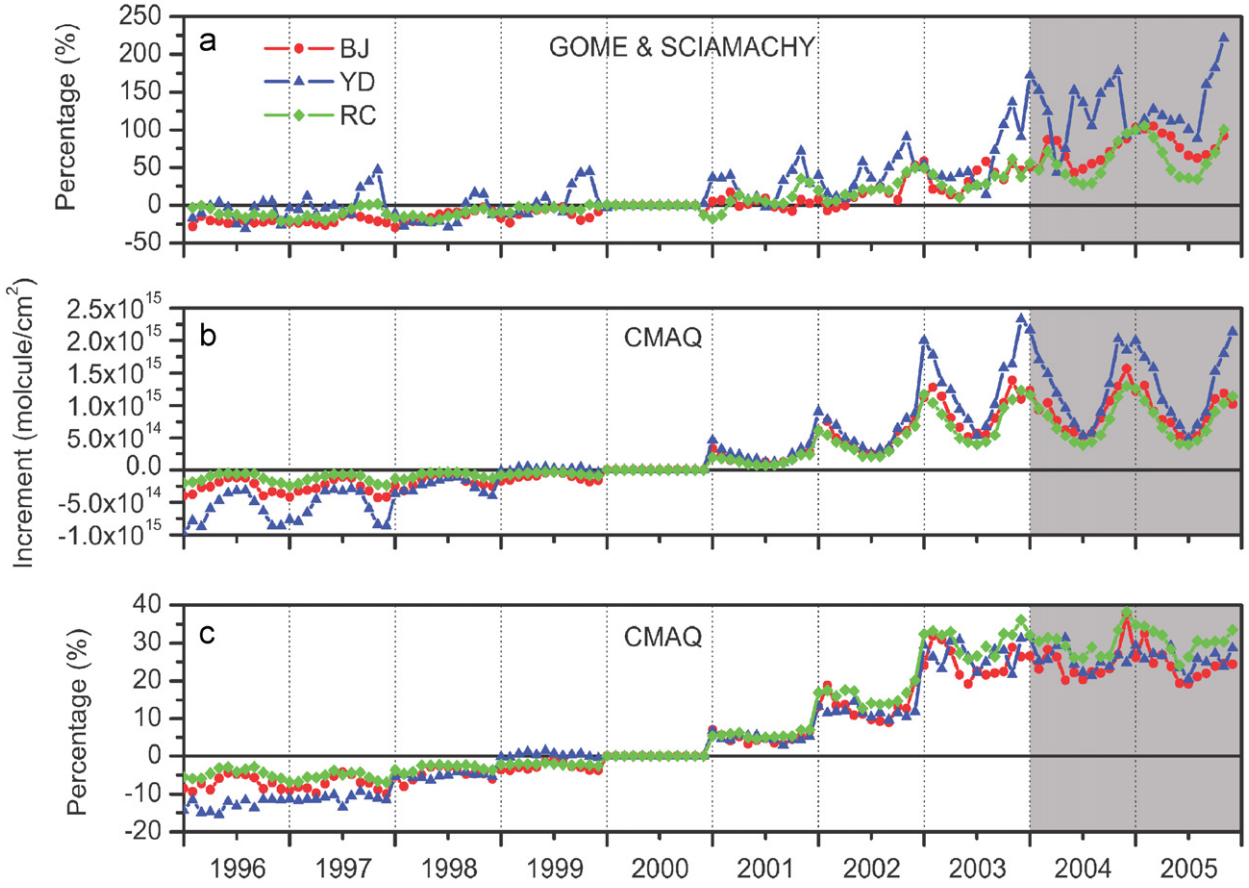

Fig. 4. Time series of the growth of NO_2 abundance (calculated by the difference from the monthly variation of NO_2 abundance of year 2000) over BJ, YD and RC during 1996–2005. (a) Increased percentage of satellite retrievals, which is shown as a 3-month moving average to reduce noise; (b) absolute increment of NO_2 abundance caused mainly by the increase in emission of model simulations and (c) increased percentage of modeled NO_2 VCDs caused chiefly by increased emission. In (a–c), the red line represents BJ, the blue line represents YD, and the green line represents RC. Model simulations with fixed emissions of 2003 for 2004–2005 are masked with shadow.

our model results, which show the highest growth rate over YD. The analysis also reveals that the satellite data indicate the highest annual growth rate of 27.5% over YD, with much faster growth of 29.0% yr^{-1} for March–November and a somewhat slower growth of 25.8% yr^{-1} for winter (December, January and February) during 2000–2005, which means that no clear seasonality of NO_2 abundance is found in YD (see Table 1). On the other hand, the satellite-measured NO_2 growth rate over BJ and RC is much higher in winter, but lower in other seasons during 2000–2005. Such a difference in the growth rate in different seasons among the three regions is also apparent in model simulations, as shown in Table 1, which might reflect that economic development patterns and the structure of energy consumption of YD is distinct from that of other regions.

Fig. 4c shows MIPE time series. The marked year-by-year jump is caused by the emission changes in the model. During 1996–2000, the MIPE in YD is much higher than that in other regions, while RC shows the highest MIPE since 2000. This feature is more readily apparent from the emission increase rate, which is shown in Table 1. The REAS inventory presents the highest rate of increase, about 11.8% yr^{-1}, over RC during 2000–2003. The model simulation (EyyMyy) also shows the highest annual increase rate of 11.5% over RC. All these data suggest that, in addition to BJ and YD, emissions from other cities and rural regions in CEC also have expanded significantly in recent years.

Overall, we attribute the difference between model simulations and satellite retrievals mainly to the underestimation of the emission inventory,

especially for BJ region. Therefore, the re-examination of the Chinese emission inventory based on the most recently updated Chinese emission-related information is important to improve the model results. This should also include the seasonal variation of emissions. At the same time, satellite retrievals are also to be examined with respect to the sharp winter peaks as shown in Fig. 2. Validations of satellite retrievals by comparing with in situ measurements are mostly taken in America or Europe, but nearly none for China. In fact, the real air pollution conditions in China may differ from that in America and Europe. Owing to the lack of enough ground-based measurements, any insufficient concern of the factors such as air mass factors, cloud fraction, aerosol concentration, surface reflectivity and so on, in the retrieval algorithm may introduce uncertainty into satellite-retrieved NO_2 VCDs. We have noticed one interesting point that an increase in sulfate aerosols can at least in principle increase the satellite measurements' sensitivity (e.g., Richter et al., 2005; van der A et al., 2006) to NO_2 which is currently not accounted for in the retrieval scheme. The REAS SO_2 emissions in China show an increase in about 30% during 2000–2003, which results in the CMAQ sulfate increase in 13% in the CEC region. Fig. 5 depicts the winter (DJF) and summer (JJA) time series of

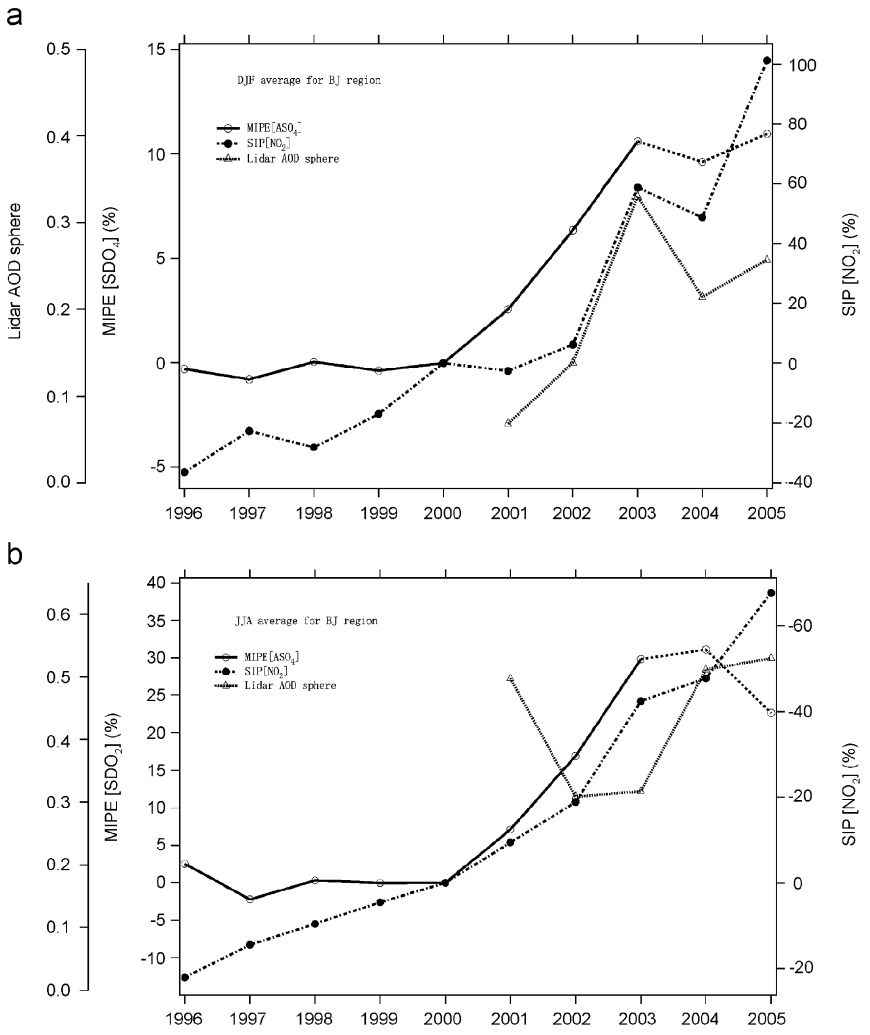

Fig. 5. Time series of the growth of modeled sulfate aerosols (MIPE[ASO_4]) and satellite-retrieved NO_2 VCDs (SIP[NO_2]) (calculated by the difference from the magnitude of year 2000, and MIPE[ASO_4] and SIP[NO_2] are defined as similar to MIPE and SIP described in Section 3.3), and lidar AOD sphere over BJ during 1996–2005. (a) Average for winter (December, January and February); (b) average for summer (June, July and August).

the increased percentage of modeled sulfate (MIPE[ASO_4]) and satellite NO_2 VCDs (SIP[NO_2]) between 1996 and 2005, based on the magnitude of year 2000. The calculation algorithm of the growth of modeled sulfate (MIPE[ASO_4]) and satellite NO_2 (SIP[NO_2]) is defined as similar to that of MIPE and SIP, which are described in Section 3.3, respectively. Sulfate aerosol is averaged below 10 km altitude from model simulations. The figures also portray the DJF and JJA average of aerosol optical depth (air pollution fraction) by NIES Mie Lidar measurement in Beijing (Shimizu et al., 2004). In Fig. 5b, the incongruous high value of lidar AOD sphere (lidar aerosol optical depth of the air pollution part) in year 2001 was examined to be mainly contributed by the near-ground high concentrations, about which the explicit reason is still unknown. Without regard of that point, lidar observations, model simulations and satellite retrievals are quite consistent both in winter and in summer. A good correlation is apparent: the regression line for the increased percentage of satellite NO_2 and modeled sulfate (year between 1996 and 2003) are

$$\mathrm{DJF}: \mathrm{SIP}[NO_2]\,(\%) = -20.05 + 6.58\ \mathrm{MIPE}\,[ASO_4]\,(\%) \quad (R = 0.91),$$

$$\mathrm{JJA}: \mathrm{SIP}[NO_2]\,(\%) = -9.16 + 1.71\ \mathrm{MIPE}\,[ASO_4]\,(\%) \quad (R = 0.92).$$

This examination suggests that the increasing sulfate could be one of the possible reasons for the striking increase in satellite retrievals during that period, both in winter and in summer. It should also be noted that the growth rate of modeled sulfate aerosol in summer is much higher than that in winter, while the increasing slope in winter is much steeper than that in summer for satellite-retrieved NO_2 VCDs. Such a phenomenon may suggest that the relationship between the increasing sulfate and satellite retrievals is nonlinear. The explicit functions of the sulfate aerosols on satellite retrievals, as well as some other unclear aspects are still not well known at present. Anyhow, detailed studies are necessary to better explore the real NO_2 abundance over CEC both from the bottom-up emission inventory and the top-down satellite retrieval algorithm sides in future.

4. Conclusions

Long-term numerical studies (between the years 1996 and 2005) using CMAQ/REAS were performed to elucidate the variation of the increasing trend of tropospheric NO_2 abundance over three parts of CEC with a comparison of GOME and SCIAMACHY retrievals during the past decade. The main conclusions are the following:

(1) GOME and SCIAMACHY observations show a continuous increase during the past decade, and with a sharp linear increase rate of 14.1–20.5% yr^{-1} after year 2000, which is almost twice as that of the Chinese GDP growth rate during 2000–2005. The variation of the increasing trend is also well reproduced by model simulations with the mild increase of 1.7% yr^{-1} before 2000 and a sharp increasing trend of 10.8% yr^{-1} for 2000–2003. In general, modeling results agree well with satellite retrievals in geographical distribution patterns, with a systematic underestimation by a factor of 1–3 for YD and RC region. For BJ, the NO_2 abundance is underestimated even more, especially in winter. The analysis indicates that REAS underestimates the emission inventory over CEC region, particularly for the BJ region.
(2) The time series of the NO_2 increase percentage (calculated by the difference from the monthly variation of NO_2 abundance of year 2000) are investigated to discuss the reasons for the variant increasing patterns over three regions in CEC. The growth rate of NO_2 abundance in YD after 2000 is higher than that of other regions, with no clear seasonal variations, both in satellite observations and in model simulations.
(3) An important finding is that the growth rate of NO_2 VCDs is definitely attributable to emission changes in RC, which are higher than that in other regions after 2000, indicating that, apart from BJ and YD, the emissions from other cities and rural regions in CEC also have expanded markedly in recent years.
(4) The underestimation of the emission inventory was examined to be mainly responsible for the difference between model results and satellite retrievals. Additionally, it was found that a high correlation exists between tropospheric sulfate aerosols and NO_2 abundance in winter, suggesting that the increased sulfate might amplify the striking increasing trend and the sharp winter peaks of satellite retrievals.

All of these findings reflect changing economic patterns and energy structure in China in recent

years, suggesting that greater attention should be devoted to environmental and climatic effects of sharply increased NO_2 emissions over the YD and RC regions.

Acknowledgments

The authors want to acknowledge Dr. Katsuya Noguchi and Prof. Sachiko Hayashida for their co-operation in satellite data analysis. Lidar data in Beijing were collected in collaboration with the Sino-Japan Friendship Center for Environmental Protection. A part of this study was supported by the European Union through ACCENT.

References

Aardenne, van J., Carmichael, A., Hiram Levy, G.R., Streets, D., Hordijk, L., 1999. Anthropogenic NO_x emissions in Asia in the period 1990–2020. Atmospheric Environment 33, 633–646.

Akimoto, H., 2003. Global air quality and pollution. Science 302, 1716–1719.

Akimoto, H., Ohara, T., Kurokawa, J., Horii, N., 2006. Verification of energy consumption in China during 1996–2003 by using satellite observational data. Atmospheric Environment 40, 7663–7667.

Boersma, K.F., Eskes, H.J., Brinksma, E.J., 2004. Error analysis for tropospheric NO_2 retrieval from space, J. Geophys. Res., 109, D04311, doi:10.1029/2003JD003962.

Burrows, J.P., Weber, M., Buchwitz, M., et al., 1999. The global ozone monitoring experiment (GOME): mission concept and first scientific results. Journal of Atmospheric Science 56, 151–175.

Heue, K.-P., Richter, Richter, A., Bruns, M., Burrow, J.P., Friedeburg, C.V., Platt, U., Pundt, I., Wang, P., Wagner, T., 2005. Validation of SCIAMACHY tropospheric NO_2-columns with AMAXDOAS measurements. Atmospheric Chemistry and Physics 5, 1039–1051.

Irie, H., Sudo, K., Akimoto, H., Richter, A., Burrows, J.P., Wagner, T., Wenig, M., Beirle, S., Kondo, Y., Sinyakov, V.P., Goutail, F., 2005. Evaluation of long-term tropospheric NO_2 data obtained by GOME over East Asia in 1996–2002. Geophysical Research Letters 32, L11810.

Kim, J., Cho, S., 2003. A numerical simulation of present and future acid deposition in North East Asia using a comprehensive acid deposition model. Atmospheric Environment 37, 3375–3383.

Kunhikrishnan, T., Lawrence, M.G., Kuhlmann, R., Richter, A., Ladstaätter-Weiβenmayer, A., Burrows, J.P., 2004. Analysis of tropospheric NO_x over Asia using the model of atmospheric transport and chemistry (MATCH-MPIC) and GOME-satellite observations. Atmospheric Environment 38, 581–596.

Leue, C., Wenig, M., Wagner, T., Oliver, K., Platt, U., Jähne, B., 2001. Quantitative analysis of NO_x emissions from GOME satellite image sequences. Journal of Geophysical Research 106, 5493–5506.

Ma, J.Z., Richter, A., Burrows, J.P., Nüβ, H., van Aardenne, J.A., 2006. Comparison of model-simulated tropospheric NO_2 over China with GOME-satellite data. Atmospheric Environment 40, 593–604.

Martin, R.V., Jacob, D.J., Chance, K., Kurosu, T.P., Palmer, P.I., Evans, M.J., 2003. Global inventory of nitrogen oxide emissions constrained by space-based observations of NO_2 columns. Journal of Geophysical Research 108 (D17), 4537.

Martin, R.V., Sioris, C.E., Chance, K., Ryerson, T.B., Bertram, T.H., Wooldridge, P.J., Cohen, R.C., Neuman, J.A., Swanson, A., Flocke, F.M., 2006. Evaluation of space-based constraints on global nitrogen oxide emissions with regional aircraft measurements over and downwind of eastern North America. Journal of Geophysical Research 111, D15308.

Ohara, et al., 2006. Overview of the REAS 1.1 emission inventory (in preparation) and at http://www.jamstec.go.jp/forsgc/research/d4/emission.htm.

Ordóñez, C., Richter, A., Steinbacher, M., Zellweger, C., Nüß, H., Burrows, J.P., Prévôt, A.S.H., 2006. Comparison of 7 years of satellite-borne and ground-based tropospheric NO_2 measurements around Milan, Italy. Journal of Geophysical Research 111, D05310.

Richter, A., Burrows, J.P., 2002. Retrieval of tropospheric NO_2 from GOME measurements. Advances in Space Research 29 (11), 1673–1683.

Richter, A., Burrows, J.P., Nüβ, H., Granier, C., Niemeier, U., 2005. Increase in tropospheric nitrogen dioxide over China observed from space. Nature 437, 129–132.

Shimizu, A., et al., 2004. Continuous observations of Asian dust and other aerosols by polarization lidars in China and Japan during ACE-Asia. Journal of Geophysical Research 109 (D19S17), 0.

Streets, D.G., Bond, T.C., Carmichael, G.R., Fernandes, S.D., Fu, Q., He, D., Klimont, Z., Nelson, S.M., Tsai, N.Y., Wand, M.Q., Woo, J.-H., Yarber, K.F., 2003. An inventory of gaseous and primary aerosol emissions in Asia in the year 2000. Journal of Geophysical Research 108 (D21), 8809.

Sudo, K., Takahashi, M., Kurokawa, J., Akimoto, H., 2002. CHASER: a global chemical model of the troposphere—1. Model description. Journal of Geophysical Research 107 (D17), 0.

Tanimoto, H., Sawa, Y., Matsueda, H., et al., 2005. Significant latitudinal gradient in the surface ozone spring maximum over East Asia. Geophysical Research Letters 32, L21805.

Uno, I., Ohara, T., Sugata, S., et al., 2005. Development of RAMS/CMAQ Asian scale chemical transport modeling system. Journal of Japan Society Atmospheric Environment 40 (4), 148–164 (in Japanese).

Uno, I., He, Y.J., Ohara, T., Yamaji, K., et al., 2007. Systematic Analysis of Interannual and Seasonal Variations of Model-simulated Tropospheric NO_2 in Asia and comparison with GOME-satellite data. Atmospheric Chemistry and Physics, accepted for publication.

van der A, R.J., Perter, D.H.M.U., Eskes, H., Boersma, K.F., Van Roozendael, M., De Smedt, I., Kelder, H.M., 2006. Detection of the trend and seasonal variation in tropospheric NO_2 over China. Journal of Geophysical Research 111, D12317.

van Noije, T.P.C., Eskes, H.J., Dentener, F.J., et al., 2006. Multi-model ensemble simulations of tropospheric NO_2 compared

with GOME retrievals for the year 2000. Atmospheric and Chemistry and Physics 6, 2943–2979.

Velders, G.J.M., Granier, C., Portmann, R.W., Pfeilsticker, K., Wenig, M., Wagner, T., Platt, U., Richter, A., Burrows, J.P., 2001. Global tropospheric NO_2 column distributions: comparing three-dimensional model calculations with GOME measurements. Journal of Geophysical Research 106 (D12), 12643–12660.